journal

J. Am. Ceram. Soc., 1–7 (2016)
DOI: 10.1111/jace.14347
© 2016 The American Ceramic Society

Low Temperature Ionic Conductivity of an Acceptor-Doped Perovskite: II. Impedance of Single-Crystal $BaTiO_3$

Russell A. Maier[‡,†] and Clive A. Randall[§]

[‡]Materials Measurement Science Division, National Institute of Standards and Technology, 100 Bureau Drive, Gaithersburg MD 20899

[§]Center for Dielectrics and Piezoelectrics, Materials Research Institute, The Pennsylvania State University, University Park, PA 16801

Low temperature conductivity mechanisms were identified in acceptor-doped $BaTiO_3$ single crystals equilibrated and quenched from high temperature under different oxygen partial pressures. A range of acceptor ionization states were quenched into samples doped with manganese or iron. Using an appropriate equivalent circuit to interpret impedance spectroscopy data, room temperature conductivity mechanisms in the single crystal samples were identified, and the permittivity/temperature dependence was also shown to be self-consistent with the nature of a first-order ferroelectric phase transition. The primary, low temperature, conduction mechanism in acceptor-doped $BaTiO_3$ was determined to be dominated by the migration of oxygen vacancies. The activation energy for oxygen vacancy migration was experimentally determined to have a value of nearly 0.7 eV. This activation energy represents an intrinsic value for vacancy hopping and confirms our previous work that revealed minimal interaction between acceptor dopants and oxygen vacancies in $BaTiO_3$ in contrast to the well-documented evidence of defect association in $SrTiO_3$.

Keywords: *impedance spectroscopy; vacancies; defects; electrical conductivity; ferroelectricity/ferroelectric materials*

I. Introduction

In practice, measuring the intrinsic conductivity of a stoichiometric, undoped oxide dielectric is a difficult task. The raw precursors used to synthesize oxide ceramics will always contain some small concentration of impurities. If the majority of impurities in the material act as acceptor dopants, the oxide will typically exhibit *p*-type conductivity, and it will have high concentrations of oxygen vacancies. Because small amounts of impurities can control the transport behavior of a perovskite material, it is important to assume that extrinsic defects control the electronic and ionic conductivity of measurements made on nominally undoped samples.[1–4] The natural abundance of elements likely to be found as impurities in the precursors used to make perovskite materials is given in Fig. 1.[5]

Figure 1 shows that there are far more naturally occurring elements that act as acceptors compared to donors in perovskite $A^{2+}B^{4+}O_3^{2-}$ chemistries. The most abundant impurities, the Group 1 Alkali metals, form large aliovalent ions that can substitute on the perovskite *A*-site. Most transition metals have ionic radii that are similar to the intrinsic size of Ti^{4+} when their valence is 4+ or less and placed in octahedral symmetry.[6] Transition metals with common valence states 5+ or greater with ionic radii similar to Ti^{4+} like Nb^{5+}, Ta^{5+}, $W^{5+/6+}$, $Mo^{5+/6+}$ that can act as *B*-site substituted donors or large rare-earth ions that can act as *A*-site donors are less common than the lighter elements that act as acceptors. In fact, the four most naturally occurring acceptor ions in order of predominance are aluminum, iron, sodium, and potassium, and even the least abundant of these four ions is found in the Earth's crust at concentrations of more than three orders of magnitude greater than one of the most common donor ions (niobium). As a result, the most common impurities in the raw materials that are used to make barium and strontium titanate will inevitably contain much more acceptors compared to donors. The effect of trace impurities on the extrinsic doping mechanism in nominally undoped, pure materials has been well documented.[1,7] Comparing the listed impurities in references[1,7] with the most abundant acceptor elements shown in Fig. 1 reveals close agreement. Unless a $A^{2+}B^{4+}O_3^{2-}$ perovskite is heavily donor doped, the material will contain many oxygen vacancies at a concentration fixed by the acceptor impurity, $2[V_O^{\bullet\bullet}] = \Delta[A_{Ti}^{\Delta}]$, where the defect concentrations are given in Kröger–Vink notation, and Δ represents the charge on the acceptor, *A*, with respect to the neutral lattice.

Oxygen vacancy mobility derived using an ionic hopping model is typically expressed as:

$$\mu_{ion} = \frac{z_i f_i q_e a_o^2 \nu_i}{6k_b T} \exp\left(\frac{\Delta S_{\text{mig}}}{k_b}\right) \exp\left(-\frac{E_A}{k_b T}\right) \quad (1)$$

with ΔS_{mig} as the ionic migration entropy, f_i the geometric factor equal to the number of oxygen nearest neighbor sites, z_i and q_e the valence and electronic charge of the ion, respectively, and the hopping attempt frequency parameter v_i is independent of temperature and should have a similar value for similar materials.[8] The value a_o is the hopping distance equal to the separation between neighboring oxygen sites. The parameters a_o, ΔS_{mig}, and E_A are dependent on local structure and should be anticipated to have discontinuous values on either side of a displacive first-order ferroelectric phase transition. However, the spontaneous strain at the cubic/tetragonal phase transition in $BaTiO_3$ is smaller compared to other ferroelectrics like $PbTiO_3$; the spontaneous strain at the phase transition in $BaTiO_3$ is 0.18% and −0.09% along the *c* and *a*-axis, respectively, as opposed to strains nearly an order of magnitude higher in $PbTiO_3$ measured at 1.3% and −0.3%.[9,10] As a result, it is expected that the small changes in lattice constants in $BaTiO_3$ at the cubic/tetragonal phase transition will result in negligible changes to the a_o terms leading to no noticeable variation in the magnitude of ionic conduction. In ionic crystals, values of ΔS_{mig} are typically on the order of a couple k_b, and

J. Stevenson—contributing editor

Manuscript No. 37677. Received October 22, 2015; approved May 8, 2016.
[†]Author to whom correspondence should be addressed. e-mail: russell.maier@nist.gov

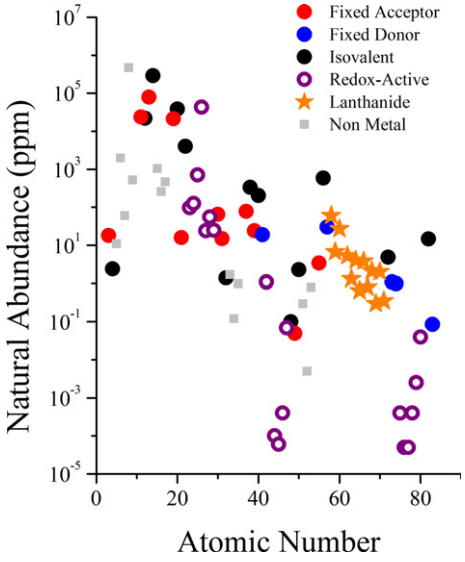

Fig. 1. The natural abundance of the first 83 elements in the Earth's crust.[5] Included are the common *A* and *B*-site fixed valence acceptor and donor dopants marked by red and blue circles, respectively, for an $A^{2+}B^{4+}O_3^{2-}$ perovskite. Elements with ionic radii larger than 90 pm in octahedral coordination were assumed to occupy the perovskite *A*-site.[5] The common acceptors include both alkali and transition-metal ions. Isovalent dopants are given as black circles. Nonmetals are marked by grey squares. Open purple circles denote transition-metal ions that are redox-active. These ions take on different valence states and are often reduced to acceptor states in materials that accommodate oxygen deficiencies. The lanthanide ions often have ionic radii intermediate between the perovskite *A* and *B*-sites. These ions can simultaneously occupy both cation sites and often act as amphoteric dopants.

comparing materials with the same structure and dissimilar lattice constants, such as NaCl and KCl, the difference in magnitude in ΔS_{mig} for vacancy hopping is negligible.[11,12] The transition from paraelectric to ferroelectric should also have an effect on the magnitude and anisotropy of the E_A term, but changes to E_A at the phase transition would need to be larger than a few meV to be experimentally observable. It should also be noted that the measurements in this study were performed on multi-domain crystals; and as a result, the measured ionic conductivity in the tetragonal phase should reflect the parallel combination of ionic conductivity through *a* and *c*-domains.

After considering the discussion of Eq. 1, it is not immediately obvious why similar perovskite systems, especially when measured at high temperature in the cubic phase, have significantly different magnitudes of ionic mobility. Based on phenomenological considerations, the predicted activation enthalpy difference for ionic migration should differ by <0.1 eV between $SrTiO_3$ and $BaTiO_3$.[13,14] In the literature however, the ionic migration enthalpy experimentally measured at high temperatures can range from 0.3 eV in $SrTiO_3$ to 2.8 eV in $BaTiO_3$.[15,16] A comprehensive list of experimentally measured values for the migration enthalpy of oxygen vacancies in $SrTiO_3$ is given in reference[17] and for $BaTiO_3$ in reference[13].

In order to determine the low temperature mobility of oxygen vacancies and to draw conclusions regarding the differences in defect association between oxygen vacancies and acceptor dopant sites in paraelectric and ferroelectric perovskite materials, the impedance responses of manganese and iron-doped $BaTiO_3$ single crystals were studied. All of the samples in this study were multi-domain <001> oriented single crystals doped with 0.5 mol% acceptor concentration and were special ordered from Ceracomp Co[1].[18] The crystals were grown using a solid-state crystal growth (SSCG) technique and were cut to dimensions of 5 × 5 × 0.5 mm. The single crystals were equilibrated at high temperature under varying oxygen activities by flowing dry N_2/H_2 gas mixtures and quenched before each impedance test was made on samples with sputtered platinum electrodes. One manganese-doped single crystal was crushed and x-ray diffraction revealed no secondary phases. Historically, $BaTiO_3$ ceramics exhibit relatively poor solubility on either side of the Ba-rich or Ti-rich stoichiometry compared to $SrTiO_3$.[19–22] Crystals grown using the SSCG method are typically slightly titania rich.[23,24] For single phase material, small deviations from perfect stoichiometry, regardless of an A/B ratio greater or less than unity, result in partial Schottky charge compensation mechanisms dominated by increases in oxygen vacancy concentration.[20] For this study, small deviations in stoichiometry should not affect the reported results because samples with large acceptor concentrations were intentionally chosen in order to test samples with large oxygen vacancy concentrations. The motivation for these room temperature conductivity experiments and details on the preparation of the samples was given in a preceeding paper.[25] It should be noted that similar work has been previously published on the conductivity of $BaTiO_3$ single crystals.[26] However, in the cited work, the conductivity was measured using dc techniques with applied fields of 1.5 kV/cm and greater. It is well-reported that moderate electric fields can result in domain wall motion at sub-coercive switching fields, and the result of this nonlinear response can have a large measureable effect on the dielectric response.[27–29] The data in this study, measured by impedance spectroscopy with maximum applied ac fields of 0.02 kV/cm, is well below the critical field above which nonlinear effects will be observed in $BaTiO_3$.[30]

II. Experimental Results

A typical complex modulus plot for a $BaTiO_3$ crystal doped with manganese is shown in Fig. 2. The real and imaginary modulus is plotted as a function of frequency in order to observe all of the relevant impedance data over a broad range of temperatures. The complex impedance data was gathered for samples equilibrated under different oxygen partial pressures at 900°C followed by quenching the samples to room temperature. The model used to fit the data was explained in detail in Part I of this series and is based on a simple electronically permeable, ionically blocking electrode,

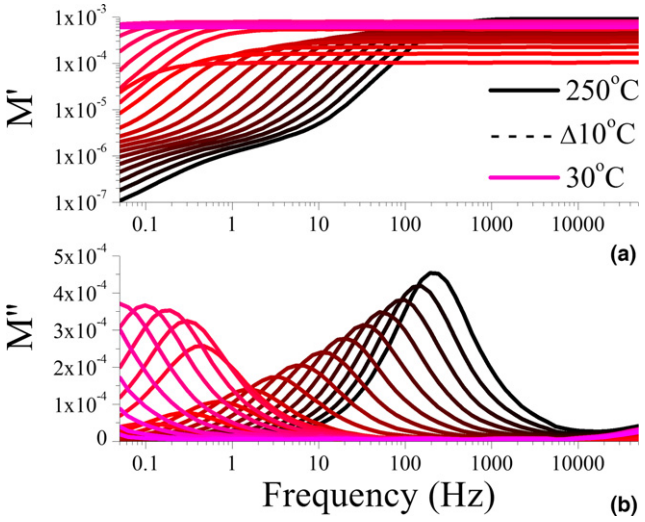

Fig. 2. The real (a) and imaginary (b) modulus of 0.5 mol% Mn-doped $BaTiO_3$ single crystal equilibrated in air at 600°C. Data are given for a range of temperatures with each temperature step equal to 10°C over a range from 30°C to 250°C.

[1]The identification of any commercial product or trade name does not imply endorsement or recommendation by the National Institute of Standards and Technology.

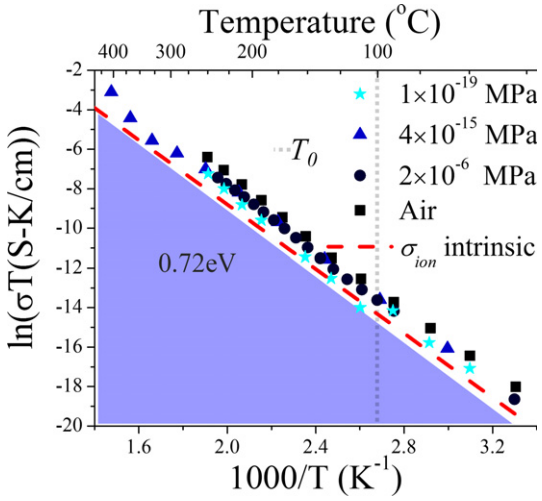

Fig. 3. The bulk conductivity of 0.5 mol% Fe-doped $BaTiO_3$ single crystals equilibrated under different oxygen activities. The intrinsic ionic conductivity was calculated using Eqs. 2 and 3 assuming 0.5 mol% acceptor concentrations of Fe'_{Ti}.

mixed conducting system.[25] This mixed conduction model has been successfully used to model conductivity in other acceptor-doped perovskite systems.[31–34]

Values of the bulk conductivity as a function of temperature for iron-doped single-crystal samples of $BaTiO_3$ are given in Fig. 3. Small anomalies in the conductivity data may be seen around the ferroelectric/paraelectric phase transition temperature, T_0, for the most reduced sample in Fig. 3. These points are artefacts of the high loss and high sensitivity to small temperature fluctuations at T_0. In addition to the experimental data in Fig. 3, the intrinsic ionic conductivity value for a system doped with 0.5 mol% iron was included.

The intrinsic ionic conductivity is calculated by considering the diffusivity of oxygen vacancies measured by Kessel et al.[13] The corrected diffusivity expression for their work is given as follows:

$$D_{V_O^{\bullet\bullet}}\left(\frac{\mathrm{cm}^2}{s}\right) = 6.4\times10^{-3}\exp\left(-\frac{0.70eV}{k_bT}\right) \tag{2}$$

The conductivity can then be predicted for a completely ionically compensated acceptor-doped system as follows:

$$\sigma_{V_O^{\bullet\bullet}} = \frac{\frac{(\Delta[A^{\Delta}])}{2}D_{V_O^{\bullet\bullet}}(z_iq_e)^2}{k_bT} \tag{3}$$

It is clear from Fig. 3 that the bulk conductivity is almost continuous through the Curie transition temperature as the sample is heated from the tetragonal to cubic phase. The discontinuous first-order phase transition is readily observed via the bulk modulus data in Fig. 2. As the conductivity is approximately continuous (within the error of the measurement) through the transition, whereas the permittivity is not, a clear discontinuity can be seen in the RC time constant in Fig. 2. The smooth transition of the bulk conductivity through the phase transition is important, because at these low measuring temperatures, the bulk conductivity is argued to be controlled by oxygen vacancy mobility given by the expression in Eq. 1.

It was stated during the discussion of Eq. 1 that effects of the ferroelectric phase transition on the intrinsic mobility parameters, a_o, ΔS_{mig}, and E_A, should be small. One further issue that potentially perturbs the ionic mobility includes the potential interactions of charge carriers with the ferroelectric domain walls.[35–37] However, because there is no noticeable anomaly in the bulk conductivity through the phase transition, it will be assumed that a majority of vacancies are not pinned by ferroelectric domains in this study. Generalizations concerning the effect of ferroelectric domains on ionic conduction will be avoided. The authors will admit that domain engineered samples with much finer sized domain configurations could have more considerable effects on the results.[38–40]

Because the $BaTiO_3$ phase transition seems to have little effect on the ionic conductivity of the sample, the large discrepancies in measured activation energy of vacancy hopping between similar lattices of $SrTiO_3$ and $BaTiO_3$ are again called into question especially considering the measurements cited in reference[13] were made at temperatures far above the tetragonal/cubic phase transition. The smooth relationship of the conductivity as it is cooled or heated through the transition temperature is also present in 0.5 mol% manganese-doped $BaTiO_3$ single crystals. The conductivity data for Mn-doped crystals equilibrated under varying degrees of oxygen activity is shown in Fig. 4. The intrinsic value of ionic conductivity is again plotted alongside the experimental data in Fig. 4 for Mn''_{Ti}-oxygen vacancy compensation, using Eqs. 2 and 3, and the close agreement between the predicted magnitude and slope should be noted.

Again, the bulk conductivity exhibits a nearly perfect Arrhenius behavior at low temperatures in the case of manganese-doped $BaTiO_3$ as in the case of iron-doped crystals. The activation energy of the conductivity should be controlled by oxygen vacancies at low temperatures in these highly acceptor-doped single crystals. As in Part I of this series, the activation energy of conductivity measured by impedance spectroscopy nearly perfectly agrees with the highly reliable values measured by isotope exchange and time-of-flight secondary ion mass spectroscopy studies conducted on both $SrTiO_3$ and $BaTiO_3$ single crystals.[13,17]

III. Discussion

Unlike the case of iron-doped $BaTiO_3$ and $SrTiO_3$, the manganese dopant results in much larger changes to the magnitude of the conductivity as a function of oxygen partial pressure during high temperature equilibration. For both the $SrTiO_3$ and $BaTiO_3$ iron-doped compositions, the color of the crystal appears to stop changing after the sample is annealed at partial pressures of 2×10^{-6} MPa or lower. The manganese-doped sample, however, continues to change

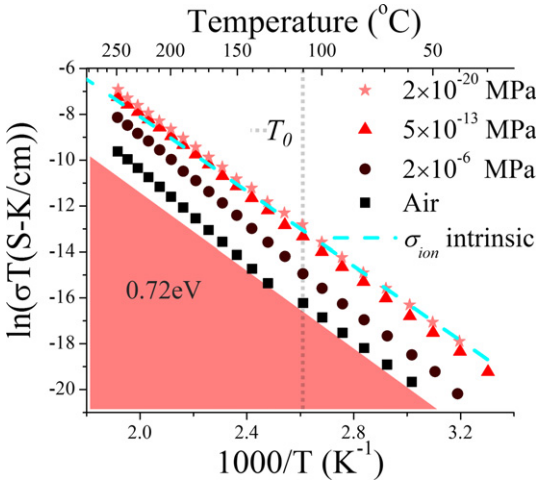

Fig. 4. The bulk conductivity for 0.5 mol% Mn-doped $BaTiO_3$ single crystals equilibrated under different oxygen activities. The intrinsic ionic conductivity was calculated using Eqs. 2 and 3 assuming 0.5 mol% acceptor concentrations of Mn''_{Ti}.

color as it is annealed under more reducing conditions. These results agree well with the transition metal ion valence state studies of doped $BaTiO_3$ made by Hagemann and Ihrig.[41] For the equilibration conditions used for the iron dopant, the ion is most often in the Fe^{3+} state at room temperature.[25,42–44] The manganese ion however, can more easily take on multiple valence states according to the following mass action reactions:

$$Mn_{Ti}^{\times} \leftrightarrow Mn_{Ti}' + h^{\bullet} \Rightarrow \frac{p[Mn_{Ti}']}{[Mn_{Ti}^{\times}]} = N_V(T)\exp\left(-\frac{E_A^1}{k_bT}\right) \tag{4}$$

$$Mn_{Ti}' \leftrightarrow Mn_{Ti}'' + h^{\bullet} \Rightarrow \frac{p[Mn_{Ti}'']}{[Mn_{Ti}']} = N_V(T)\exp\left(-\frac{E_A^2}{k_bT}\right) \tag{5}$$

where $N_V(T)$ is the density of states in the valence band and E_A^1 and E_A^2 are the ionization energies of the Mn^{3+}/Mn^{4+} and Mn^{2+}/Mn^{3+} transitions, respectively. These ionization energies were measured by Hagemann and collected by Wechsler and Klein for $BaTiO_3$ ceramics.[45] The ionization values for the E_A^1 and E_A^2 transitions for manganese in the $BaTiO_3$ lattice are 1.3 eV and 1.9 eV, respectively, and 0.8 eV and 2.4 eV for the equivalent transitions for iron. The effect each dopant has on the conductivity of the single crystals measured in Figs. 3 and 4 can be estimated using Eqs. (4) and (5) with the additional mass action equations given in Part I of this series for $SrTiO_3$.

There are plenty of studies available in the literature where the mass action constants have been calculated for the $BaTiO_3$ system; however, the mass action values for the oxygen reduction equation, band gap, density of states, and electron and hole mobilities are similar in magnitude to the $SrTiO_3$ system.[46] The mass action equations given by Moos and Härdtl in Part I of this series are preferred because they have included the temperature dependence of the density of states as well as the band gap.[47] Using these defect equations along with Eqs. 4 and 5, the normalized oxygen vacancy concentration was calculated for samples with 0.5 mol% dopant equilibrated and quenched from 900°C as a function of oxygen partial pressure and plotted in Fig. 5. The average measured conductivity, normalized to the conductivity of samples equilibrated in air, at temperatures below 200°C for the manganese and iron-doped $BaTiO_3$ data in Figs. 3 and 4 is included in Fig. 5. The ionization energies of Eqs. 4 and 5 will be assumed to constitute relative values. These energies tend to have a large range in the literature.[45,48,49] To compensate for this uncertainty, the value of the $3^+/4^+$ transition calculated by Hagemann was fixed, and the $2^+/3^+$ ionization energy was allowed to take on a range of values in Fig. 5. The data was plotted in this manner to illustrate the relative effect the difference in energy between these two transitions has on the quenched concentration of oxygen vacancies in the system.

For the iron-doped system, the large ionization energy for the $2^+/3^+$ transition requires $[Fe_{Ti}'] = 2[V_O^{\bullet\bullet}]$ to be the dominant charge compensation mechanism at 900°C regardless of the oxygen partial pressure. Exhausting the maximum acceptor compensation for a manganese-doped material takes a much broader range of oxygen partial pressures than it does for the iron-doped system as both manganese valence states are energetically available at the temperatures used in this study $[Mn_{Ti}'] + 2[Mn_{Ti}''] = 2[V_O^{\bullet\bullet}]$. As can be seen in Fig. 4, saturation of the oxygen vacancy concentration, and thus frozen-in ionic conductivity at low temperatures, is approached near 10^{-18} MPa p_{O_2} at temperatures of 900°C for the manganese system.

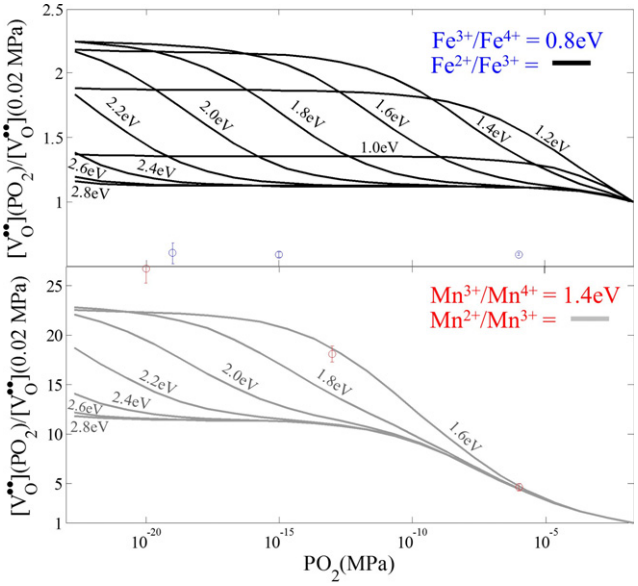

Fig. 5. Normalized equilibrium oxygen vacancy concentration for iron and manganese-doped $BaTiO_3$ at 900°C. The vacancy concentrations are normalized to the equilibrium concentration at 0.02 MPa. The open circles were calculated from Figs. 3 and 4 and represent the conductivity ratio $\sigma(p_{O_2})/\sigma(\text{air})$ at temperatures below 200°C.

In addition to fitting the complex impedance data of the $BaTiO_3$ samples in order to extract the bulk conductivity values, the static dielectric permittivity can also be calculated from the fit of the high frequency impedance. In order to demonstrate the appropriateness of the equivalent circuit model used to fit the impedance data, the static dielectric constant calculated from the fit of the impedance data is plotted as a function of temperature in Fig. 6. The data in Fig. 6 agrees well with the expected permittivity data for $BaTiO_3$ as function of temperature through the paraelectric/ferroelectric transition.[50] The data also exhibits a typical shift in the Curie temperature as a function of equilibration atmosphere for the manganese-doped samples. This same type of dependence of Curie temperature on acceptor ionization state has been observed in similar aged samples doped with iron and manganese.[41,51]

In addition to the permittivity data plotted in Fig. 6, the fit of the impedance data can be checked against the required Curie–Weiss behavior that should be observed in the ferroelectric crystals. The Curie–Weiss law is given as follows:

$$\varepsilon_r - 1 = \frac{C}{T - T_0} \tag{6}$$

where C is the Curie constant and T_0 is the Curie temperature. A plot of inverse permittivity, $1/\varepsilon_r$, versus absolute temperature should result in a linear relationship with a slope equal to the Curie constant and intercept at the y-axis equivalent to T_0. This relationship for the data in Fig. 6 is plotted in Fig. 7. The Curie constant and T_0 for the fitted data in Fig. 7 are presented in Table I.

A large shift in T_0 as a function of oxygen activity is confirmed in the manganese-doped samples. In the previously mentioned study, a shift in T_0 of approximately 15°C is seen for similar dopant concentrations (0.5 mol% Mn) in $BaTiO_3$ samples annealed in oxygen compared to samples annealed in hydrogen mixtures while minimal shifts in T_0 are seen for iron-doped samples similar to the results presented in Table I.[41] Higher reduction conditions result in a shift of the T_0 to lower temperatures away from the intrinsic value of an undoped sample around 127°C.[52] Even though the T_0 of the

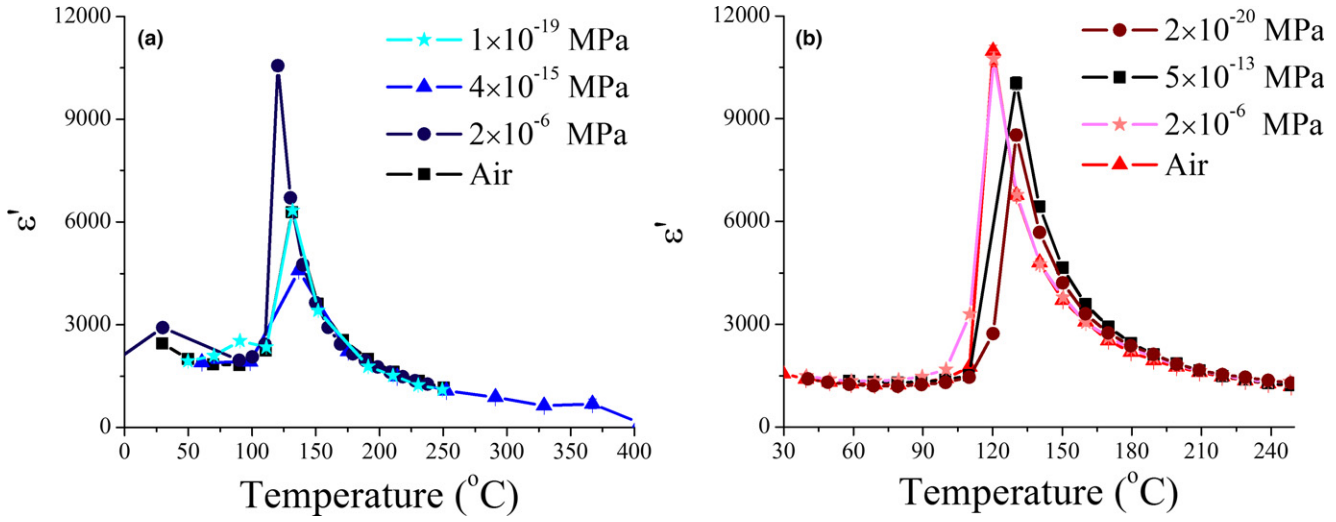

Fig. 6. The fitted permittivity data extracted from the complex impedance measured on (a) 0.5 mol% Fe-doped $BaTiO_3$ and (b) 0.5 mol% Mn-doped $BaTiO_3$.

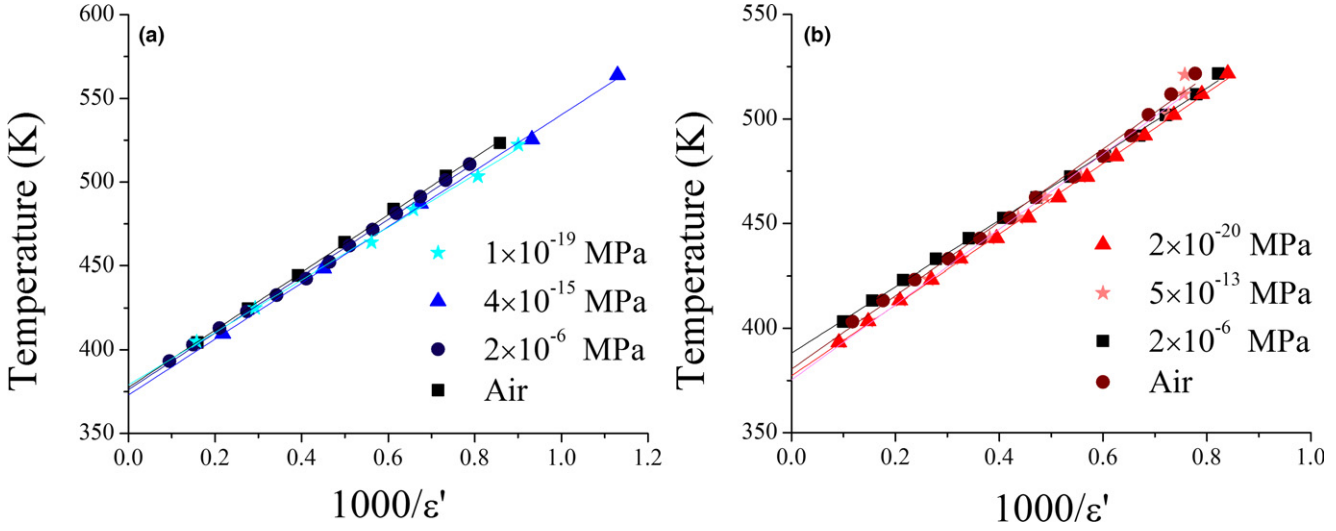

Fig. 7. Fits of the data in Figure 5 to the Curie–Weiss law for (a) 0.5 mol% Fe-doped $BaTiO_3$ and (b) 0.5 mol% Mn-doped $BaTiO_3$.

Table I. Curie–Weiss Fit Parameters with the Standard Uncertainty of the Experimentally Observed Values for Fe and Mn Single Crystal Samples Equilibrated Under Various p_{O_2} Conditions

Fe annealing condition (atm)				
	0.2	2×10^{-5}	4×10^{-4}	1×10^{-18}
T_0 (°C)	104 ± 1	103 ± 1	100 ± 2	106 ± 2
C ($\times 10^4$°C)	17.2 ± 0.2	16.9 ± 0.2	16.7 ± 0.3	15.7 ± 0.4
Mn annealing condition (atm)				
	0.2	2×10^{-5}	5×10^{-12}	2×10^{-19}
T_0 (°C)	115 ± 1	107 ± 2	104 ± 1	102 ± 2
C ($\times 10^4$°C)	15.8 ± 0.2	17.5 ± 0.4	16.9 ± 0.1	18.0 ± 0.4

iron-doped crystal shows a negligible dependence on oxygen activity, the T_0 value is measured at a much lower temperature than that of intrinsic $BaTiO_3$. The manganese-doped samples, in fact, approach the values of the iron-doped samples under strong reducing conditions.

The effect of impurity acceptor ions on the displacement of the intrinsic T_0 has been previously explained by K.A. Muller.[53] In summation, the Fe^{3+} and Mn^{2+} ions remain centered in the oxygen octahedron and do not participate in ferroelectric displacements. The larger the concentration of Fe^{3+} or Mn^{2+} in the sample, the larger the volume of crystalline regions in the sample that do not take part in the collective spontaneous polarization of the ferroelectric phase. As was shown from the impedance data, the iron-doped samples are all nearly saturated with Fe^{3+} regardless of the preparation conditions, whereas the manganese-doped samples require low p_{O_2} reduction conditions to saturate the concentration of Mn^{2+}. These observations are typical of other reported results for acceptor-doped $BaTiO_3$ materials and are indicative of an acceptor ion substituted on the *B*-site of perovskite lattice surrounded by a full oxygen octahedron.[41,50,53]

As described using Fig. 1, impurities in the precursor oxide materials make the likelihood of being able to

synthesize a truly undoped sample small. The acceptor dopant concentration fixes the large oxygen vacancy concentrations during processing or subsequent equilibration processes, and the slow surface reoxidation kinetics limits the ability of the single crystal samples to undergo the necessary redox reactions required to oxidize the acceptor dopants to the room temperature neutral states ($A_{Ti}^{\times}$). For the temperature ranges considered in this study, it was shown in Part I that the activation energy of the bulk conductivity of $SrTiO_3$ or $BaTiO_3$ should be controlled by the ionic mobility or the concentration of holes which has an activation energy given by the mass action Eqs. 4 and 5.

The activation energy for bulk conductivity was found to be the same for both manganese and iron-doped $BaTiO_3$ in this study, and the acceptor ionization energies for these two dopants have been shown to have significantly higher values than the low bulk conductivity activation energy of nearly 0.7 eV measured for both $BaTiO_3$ and $SrTiO_3$.[45] This 0.7 eV activation energy value for oxygen vacancy hopping has recently been measured by tracer diffusion in $BaTiO_3$ using oxygen isotope exchange with time-of-flight secondary ion mass spectroscopy TOF-SIMS.[13] The range of reported activation energies for oxygen vacancy hopping is expansive as previously discussed. Most of the reported values that are >1.0 eV were measured at high temperatures where the ionic conductivity is the minority component of the total bulk conductivity.[54,55] In these cited studies, the extrinsic contribution of impurity transition metal defects in the system is difficult to control or account for partially because the ionization energies for deeper impurity valence states not typically seen in samples measured at room temperature are energetically accessible at high temperatures. The oxygen isotope exchange TOF-SIMS experiments are able to avert both of these experimental complications because: (1) the ionic component of the measured response does not need to be separated from an electronic component, and (2) if proper care is taken, the negative effects of impurities on the analysis of vacancy mobility can be avoided with isotope exchange experiments. To clarify, the tracer diffusivity measured by isotope exchange diffusion experiments is a function of both the vacancy diffusivity and concentration of the oxygen vacancies. Therefore, the enthalpy of migration for the tracer is[17]:

$$\Delta H_{D^*} = \frac{d\ln\left(D_{V_O^{\bullet\bullet}}\right)}{d\left(\frac{1}{k_b T}\right)} - \frac{d\ln\left([V_O^{\bullet\bullet}]\right)}{d\left(\frac{1}{k_b T}\right)} \tag{7}$$

If a sample has redox-active impurities, the vacancy concentration will decrease as the sample is cooled from high temperatures; and according to Eq. 7, this change in concentration will have an additive effect on the measured tracer enthalpy of migration. The exclusion of redox-active impurities from the defect chemical models of perovskite conductivity may explain the erroneously large values measured by other researchers. However, for isotope exchange measurements, if the concentration of redox-active impurities is less than the concentration of impurities with fixed valence, the vacancy concentration will remain fixed over the measurement temperature range. In both isotope exchange studies cited in this work, proper care was taken to analyze the impurity concentrations. In the $SrTiO_3$ work, the major impurities were determined to be fixed valence acceptors Al'_{Ti} and Mg''_{Ti}, and in the $BaTiO_3$ work, the major impurities were determined to be Zn''_{Ti}.[13,17] As a result, these studies on single crystals systems should represent the most accurate measurement of intrinsic oxygen vacancy mobility in $SrTiO_3$ and $BaTiO_3$.[13,17]

By equilibrating appropriately acceptor-doped $SrTiO_3$ and $BaTiO_3$ single crystals, high ionic transference can be quenched to low temperatures allowing the activation energy of the bulk conductivity to represent the barrier for oxygen vacancy hopping. The activation energies measured by Kessel et al. and De Souza et al. should represent the lower limit for the activation energy of bulk conductivity in $SrTiO_3$ and $BaTiO_3$. If larger activation energies are measured in quenched, acceptor-doped systems, the interaction of oxygen vacancies with acceptor defect centers may impact the effective vacancy mobility at low temperatures. Recently, the effect of defect complex formation on the mobility of oxygen vacancies was theoretically calculated for a few common transition-metal impurities.[56] Nickel was shown to have the biggest impact on oxygen vacancy migration in $SrTiO_3$, increasing the effective barrier for hopping to nearly 1 eV from the intrinsic value of 0.62 eV. This high activation energy has been measured experimentally in quenched $SrTiO_3$ samples doped with nickel.[57] The formation of defect complexes in nickel-doped $SrTiO_3$ single crystals of the form $\left(Ni'_{Ti} - V_O^{\bullet\bullet}\right)^{\bullet}$ has also be confirmed with electron paramagnetic resonance (EPR) measurements.[58] The activation energy of 0.59-0.78 eV measured in iron-doped $SrTiO_3$ in Part I of this study is higher than the intrinsic value of 0.62 eV.[17] Defect complexes of $\left(Fe'_{Ti} - V_O^{\bullet\bullet}\right)^{\bullet}$ have also been proven to form at low temperatures in $SrTiO_3$ single crystals, so these results (the low temperature ionic conductivity in nickel-doped $SrTiO_3$ has a significantly higher activation energy than that of iron-doped $SrTiO_3$) suggest that the association energy for iron related defect complexes is smaller than that of nickel complexes.[59,60] Unlike the $SrTiO_3$ system, it has been shown in a recent study, that defect complexes between oxygen vacancies and manganese dopants are not the majority point defects in the $BaTiO_3$ system; most of the charge compensating oxygen vacancy defects are *free* and do not form a defect complex.[50] Additionally, the $\left(Fe'_{Ti} - V_O^{\bullet\bullet}\right)^{\bullet}$ defect complex has only been observed by EPR in $BaTiO_3$ in one study and only at low temperature in the rhombohedral phase.[61] There are additional published claims of the $\left(Fe'_{Ti} - V_O^{\bullet\bullet}\right)^{\bullet}$ complex characterized by EPR in the literature; however, these studies have major flaws that include making measurements on crystals that have a cubic/tetragonal phase transition at 20°C as well as making measurements on polycrystalline iron-doped $BaTiO_3$ in which the characterization of the EPR signal as that of $\left(Fe'_{Ti} - V_O^{\bullet\bullet}\right)^{\bullet}$ should be questioned.[62–64] As shown in Figs. 3 and 4, the activation energy for vacancy migration is identical in iron and manganese-doped $BaTiO_3$, and this value agrees with the intrinsic value of 0.7 eV measured by TOF-SIMS.[13] These results from conductivity measurements support the observation that $\left(Fe'_{Ti} - V_O^{\bullet\bullet}\right)^{\bullet}$ and $\left(Mn''_{Ti} - V_O^{\bullet\bullet}\right)^{\times}$ defect complexes are minority defects in $BaTiO_3$ in the tetragonal and cubic phases and do not affect the oxygen vacancy sublattice in a similar manner seen in $SrTiO_3$. The reason defect complexes form readily in the $SrTiO_3$ lattice but not in $BaTiO_3$ is still not understood and deserves further attention.

IV. Conclusions

Acceptor-doped ferroelectric $BaTiO_3$ samples were shown to exhibit low temperature conductivity dominated by oxygen vacancy migration. The transition from cubic to tetragonal symmetry resulted in negligible changes to the vacancy mobility. The similarity in structures and lattice constants between the two $SrTiO_3$ and $BaTiO_3$ systems suggests an ionic hopping conduction mechanism should result in similar activation energies for both perovskites. The data presented in this study offers strong evidence to support the idea that both systems share complementary ionic conductivity behavior at low temperatures. The primary difference between the two perovskites is the definite tendency for $SrTiO_3$ to form oxygen vacancy defect complexes at low temperatures, whereas this driving force for defect association in $BaTiO_3$ is not as strong resulting in a temperature and acceptor concentration-dependent vacancy mobility expression for $SrTiO_3$ and a classic temperature-independent expression suitable for $BaTiO_3$.

Acknowledgments

This material is based upon work supported by the National Science Foundation, as part of the Center for Dielectric Studies under Grant No. 0628817 and by the Air Force under Grant No. FA9550-14-1-0067.

References

[1]N.-H. Chan, R. K. Sharma, and D. M. Smyth, "Nonstoichiometry in $SrTiO_3$," *J. Electrochem. Soc.*, **128** [8] 1762–9 (1981).
[2]D. M. Smyth, "The Role of Impurities in Insultating Transition Metal Oxides," *Prog. Solid State Chem.*, **15** [3] 145–71 (1984).
[3]D. Smyth, "The Effects of Dopants on the Properties of Metal Oxides," *Solid State Ionics*, **129** [1–4] 5–12 (2000).
[4]C. A. Randall, R. Maier, W. Qu, K. Kobayashi, K. Morita, et al., "Improved Reliability Predictions in High Permittivity Dielectric Oxide Capacitors Under High dc Electric Fields with Oxygen Vacancy Induced Electromigration," *J. Appl. Phys.*, **113** [1] 014101 (2013).
[5]K. Hans Wedepohl, "The Composition of the Continental Crust," *Geochim. Cosmochim. Acta*, **59** [7] 1217–32 (1995).
[6]R. D. Shannon and C. T. Prewitt, "Effective Ionic Radii in Oxides and Fluorides," *Acta Crystallogr. Sect. B Struct. Crystallogr. Cryst. Chem*, **25** [5] 925–46 (1969).
[7]N.-H. Chan, R. K. Sharma, and D. M. Smyth, "Nonstoichiometry in Undoped $BaTiO_3$," *J. Am. Ceram. Soc.*, **64** [9] 556–62 (1981).
[8]D. M. Smyth, *The Defect Chemistry of Metal Oxides*, 1st edn. Oxford University Press, New York, 2000.
[9]H. D. Megaw, "Temperature Changes in the Crystal Structure of Barium Titanium Oxide," *Proc. R. Soc. London Ser. A-Mathematical Phys. Sci*, **189** [1017] 261–83 (1947).
[10]S. A. Mabud and A. M. Glazer, "Lattice Parameters and Birefringence in $PbTiO_3$ Single Crystals," *J. Appl. Cryst*, **12**, 49–53 (1979).
[11]J. Maier, "Defect Chemistry: Composition, Transport, and Reactions in the Solid State; Part I: Thermodynamics," *Angew. Chem. Int. Ed. Engl.*, **32** [3] 313–456 (1993).
[12]R. W. Dreyfus and A. S. Nowick, "Energy and Entropy of Formation and Motion of Vacancies in NaCl and KCl Crystals," *J. Appl. Phys.*, **33** [1] 473–7 (1962).
[13]M. Kessel, R. A. De Souza, and M. Martin, "Oxygen Diffusion in Single Crystal Barium Titanate," *Phys. Chem. Chem. Phys.*, **17** [19] 12587–97 (2015).
[14]J. A. Kilner and R. J. Brook, "A Study of Oxygen Ion Conductivity in Doped Non-Stoichiometric Oxides," *Solid State Ionics*, **6** [3] 237–52 (1982).
[15]L. C. Walters and R. E. Grace, "Diffusion of Point Defects in Strontium Titanate," *J. Phys. Chem. Solids*, **28** [2] 245–8 (1967).
[16]A. Muller and K. H. Hardtl, "Ambipolar Diffusion Phenomena in $BaTiO_3$ and $SrTiO_3$," *Appl. Phys. A Solids Surfaces*, **49** [1] 75–82 (1989).
[17]R. A. De Souza, V. Metlenko, D. Park, and T. E. Weirich, "Behavior of Oxygen Vacancies in Single-Crystal $SrTiO_3$: Equilibrium Distribution and Diffusion Kinetics," *Phys. Rev. B*, **85** [17], 174109 (2012).
[18]S.-J. L. Kang, J.-H. Park, S.-Y. Ko, and H.-Y. Lee, "Solid-State Conversion of Single Crystals: The Principle and the State-of-the-Art," *J. Am. Ceram. Soc.*, **98** [2] 347–60 (2015).
[19]R. K. Sharma, N. Chan, and D. M. Smyth, "Solubility of TiO_2 in $BaTiO_3$," *J. Am. Ceram. Soc.*, **64** [8] 448–51 (1981).
[20]S. Witek and D. M. Smyth, "Variability of the Sr/Ti Ratio in $SrTiO_3$," *J. Am. Ceram. Soc.*, **67** [5] 372–5 (1984).
[21]S. Lee, C. A. Randall, and Z.-K. Liu, "Comprehensive Linkage of Defect and Phase Equilibria Through Ferroelectric Transition Behavior in $BaTiO_3$-Based Dielectrics: Part 2. Defect Modeling Under Low Oxygen Partial Pressure Conditions," *J. Am. Ceram. Soc.*, **91** [6] 1753–61 (2008).
[22]S. Lee, C. A. Randall, and Z.-K. Liu, "Modified Phase Diagram for the Barium Oxide-Titanium Dioxide System for the Ferroelectric Barium Titanate," *J. Am. Ceram. Soc.*, **90** [8] 2589–94 (2007).
[23]W. Rheinheimer, M. Baurer, and M. J. Hoffmann, "A Reversible Wetting Transition in Strontium Titanate and its Influence on Grain Growth and the Grain Boundary Mobility," *Acta Mater.*, **101**, 80–9 (2015).
[24]S. Y. Choi, S. J. L. Kang, S. Y. Chung, T. Yamamoto, and Y. Ikuhara, "Change in Cation Nonstoichiometry at Interfaces During Crystal Growth in Polycrystalline $BaTiO_3$," *Appl. Phys. Lett.*, **88** [1] 86–9 (2006).
[25]R. A. Maier and C. A. Randall, "Low Temperature Ionic Conductivity of an Acceptor Doped Perovskite: I. Impedance of Single Crystal $SrTiO_3$," *J. Am. Ceram. Soc.*, in press (2016).
[26]A. Branwood and R. H. Tredgold, "The Electrical Conductivity of Barium Titanate Single Crystals," *Proc. Phys. Soc*, **76** [1] 93–8 (1960).
[27]A. Pramanick, A. D. Prewitt, J. S. Forrester, and J. L. Jones, "Domains, Domain Walls and Defects in Perovskite Ferroelectric Oxides: A Review of Present Understanding and Recent Contributions," *Crit. Rev. Solid State Mater. Sci.*, **37** [4] 243–75 (2012).
[28]D. Damjanovic and M. Demartin, "Contribution of the Irreversible Displacement of Domain Walls to the Piezoelectric Effect in Barium Titanate and Lead Zirconate Titanate Ceramics," *J. Phys. Condens. Matter*, **9** [23] 4943–53 (1999).
[29]D. Damjanovic and M. Demartin, "The Rayleigh Law in Piezoelectric Ceramics," *J. Phys. D Appl. Phys.*, **29** [7] 2057–60 (1999).
[30]D. A. Hall, "Nonlinearity in Piezoelectric Ceramics," *J. Mater. Sci.*, **36** [19] 4575–601 (2001).
[31]F. Noll, W. Munch, I. Denk, and J. Maier, "$SrTiO_3$ as a Prototype of a Mixed Conductor Conductivities, Oxygen Diffusion and Boundary Effects," *Solid State Ionics*, **86–88** [2] 711–7 (1996).
[32]J. Jamnik, J. Maier, and S. Pejovnik, "A Powerful Electrical Network Model for the Impedance of Mixed Conductors," *Electrochim. Acta*, **44**, 4139–45 (1999).
[33]J. Jamnik and J. Maier, "Generalised Equivalent Circuits for Mass and Charge Transport: Chemical Capacitance and its Implications," *Phys. Chem. Chem. Phys.*, **3** [9] 1668–78 (2001).
[34]N. J. Donnelly and C. A. Randall, "Mixed Conduction and Chemical Diffusion in a $Pb(Zr_{0.53},Ti_{0.47})O_3$ Buried Capacitor Structure," *Appl. Phys. Lett.*, **96** [5] 052906 (2010).
[35]A. Chandrasekaran, X.-K. Wei, L. Feigl, D. Damjanovic, N. Setter, et al., "Asymmetric Structure of 90° Domain Walls and Interactions with Defects in $PbTiO_3$," *Phys. Rev. B*, **93** [14] 144102 (2016).
[36]A. K. Tagantsev, L. E. Cross, and J. Fousek, *Domains in Ferroic Crystals and Thin Films, 1st ed.* Springer, New York, NY, 2010.
[37]N. Bassiri-Gharb, I. Fujii, E. Hong, S. Trolier-Mckinstry, and D. V. Taylor, et al., "Domain Wall Contributions to the Properties of Piezoelectric Thin Films," *J. Electroceramics*, **19** [1] 47–65 (2007).
[38]N. Luo, S. Zhang, Q. Li, Q. Yan, and Y. Zhang, et al., "Crystallographic Dependence of Internal Bias in Domain Engineered Mn-Doped Relaxor-$PbTiO_3$ Single Crystals," *J. Mater. Chem. C*, **4** [20], 4568–76 (2016).
[39]P. S. Bednyakov, T. Sluka, A. K. Tagantsev, D. Damjanovic, and N. Setter, "Formation of Charged Ferroelectric Domain Walls with Controlled Periodicity," *Sci. Rep.*, **5**, 15819 (2015).
[40]T. Sluka, A. K. Tagantsev, P. Bednyakov, and N. Setter, "Free-Electron Gas at Charged Domain Walls in Insulating $BaTiO_3$," *Nat. Commun.*, **4**, 1808 (2013).
[41]H. J. Hagemann and H. Ihrig, "Valence Change and Phase Stability of 3d-Doped $BaTiO_3$ Annealed in Oxygen and Hydrogen," *Phys. Rev. B*, **20** [9] 3871–8 (1979).
[42]T. Bieger, J. Maier, and R. Waser, "Optical Investigation of Oxygen Incorporation in $SrTiO_3$," *Solid State Ionics*, **53–56**, 578–82 (1992).
[43]T. Bieger, J. Maier, and R. Waser, "An Optical In-Situ Method to Study Redox-Kinetics in $SrTiO_3$," *Berichte der Bunsengesellschaft für Phys. Chemie*, **97** [9] 1098–104 (1993).
[44]R. Waser, T. Bieger, and J. Maier, "Determination of Acceptor Concentrations and Energy Levels in Oxides Using an Optoelectronic Technique," *Solid State Commun.*, **76** [8] 1077–81 (1990).
[45]B. A. Wechsler and M. B. Klein, "Thermodynamic Point Defect Model of $BaTiO_3$ and Application to the Photorefractive Effect," *J. Opt. Soc. Am. B-Optical Phys*, **5**, 1711–23 (1988).
[46]H.-I. Yoo, C.-R. Song, and D.-K. Lee, "$BaTiO_{3-\delta}$: Defect Structure, Electrical Conductivity, Chemical Diffusivity, Thermoelectric Power, and Oxygen Nonstoichiometry," *J. Electroceramics*, **8** [1] 5–36 (2002).
[47]R. Moos and K. H. Hardtl, "Defect Chemistry of Donor-Doped and Undoped Strontium Titanate Ceramics between 1000° and 1400°C," *J. Am. Ceram. Soc.*, **80** [10] 2549–62 (1997).
[48]J. Kim, C. Song, and H. Yoo, "Mn-doped $BaTiO_3$: Electrical Transport Properties in Equilibrium State," *J. Electroceramics*, **1** [1] 27–39 (1997).
[49]M. Nakahara and T. Murakami, "Electronic States of Mn Ions in $Ba_{0.97}Sr_{0.03}O_3$ Single Crystals," *J. Appl. Phys.*, **45** [9] 3795–800 (1974).
[50]R. A. Maier, T. A. Pomorski, P. M. Lenahan, and C. A. Randall, "Acceptor-Oxygen Vacancy Defect Dipoles and Fully Coordinated Defect Centers in a Ferroelectric Perovskite Lattice : Electron Paramagnetic Resonance Analysis of Mn^{2+} in Single Crystal $BaTiO_3$," *J. Appl. Phys.*, **118** [16], 164102 (2015).
[51]P. V Lambeck and G. H. Jonker, "The Nature of Domain Stabilization in Ferroelectric Perovskites," *J. Phys. Chem. Solids*, **47** [5] 453–61 (1986).
[52]S. Lee, Z. K. Liu, M. H. Kim, and C. A. Randall, "Influence of Nonstoichiometry on Ferroelectric Phase Transition in $BaTiO_3$," *J. Appl. Phys.*, **101** [5] 054119 (2007).
[53]E. Siegel and K. A. Muller, "Local Position of Fe^{3+} in Ferroelectric $BaTiO_3$," *Phys. Rev. B*, **20** [9] 3587–96 (1979).
[54]C. J. Shin, H. I. Yoo, and C. E. Lee, "Al-Doped $SrTiO_3$: Part I, Anomalous Oxygen Nonstoichiometry," *Solid State Ionics*, **178** [15–18] 1081–7 (2007).
[55]N.-H. Chan, R. K. Sharma, and D. M. Smyth, "Nonstoichiometry in Acceptor-Doped $BaTiO_3$," *J. Am. Ceram. Soc.*, **65** [3] 167–70 (1982).
[56]M. Schie, R. Waser, and R. A. De Souza, "A Simulation Study of Oxygen-Vacancy Behavior in Strontium Titanate: Beyond Nearest-Neighbor Interactions," *J. Phys. Chem. C*, **118** [28] 15185–92 (2014).
[57]R. Waser, "Bulk Conductivity and Defect Chemistry of Acceptor-Doped Strontium Titanate in the Quenched State," *J. Am. Ceram. Soc.*, **74** [8] 1934–40 (1991).
[58]K. A. Müller, W. Berlinger, and R. S. Rubins, "Observation of Two Charged States of a Nickel-Oxygen Vacancy Pair in $SrTiO_3$ by Paramagnetic Resonance," *Phys. Rev.*, **186** [2] 361–71 (1969).
[59]E. Siegel and K. A. Muller, "Structure of Transition-Metal-Oxygen-Vacancy Pair Centers," *Phys. Rev. B*, **19** [1] A109–20 (1979).
[60]E. S. Kirkpatrick, K. A. Muller, and R. S. Rubins, "Strong Axial Electron Paramagnetic Resonance Spectrum of Fe^{3+} in $SrTiO_3$ Due to Nearest-Neighbor Charge Compensation," *Phys. Rev.*, **135** [1A] A86–90 (1964).
[61]E. Possenriede, O. F. Schirmer, H. J. Donnerberg, G. Godefroy, and A. Maillard, "ESR Identification of Fe Containing Defects in $BaTiO_3$," *Ferroelectrics*, **92**, 245–52 (1989).
[62]D. J. A. Gainon, "EPR Observation of Oxygen Vacancies in Iron-Doped BaTiO3," *J. Appl. Phys.*, **36** [7] 2325–6 (1965).
[63]W. L. Warren, K. Vanheusden, D. Dimos, G. E. Pike, and B. A. Tuttle, "Oxygen Vacancy Motion in Perovskite Oxides," *J. Am. Ceram. Soc.*, **79** [2] 536–8 (1996).
[64]W. L. Warren, G. E. Pike, K. Vanheusden, D. Dimos, B. A. Tuttle, and J. Robertson, "Defect-Dipole Alignment and Tetragonal Strain in Ferroelectrics," *J. Appl. Phys.*, **79** [12] 9250–7 (1996). □